

Article

The Free-Energy Landscape of a Mechanically Bistable DNA Origami

Chak Kui Wong  and Jonathan P. K. Doye * 

Physical and Theoretical Chemistry Laboratory, Department of Chemistry, University of Oxford,
South Parks Road, Oxford OX1 3QZ, UK; chak.wong@some.ox.ac.uk

* Correspondence: jonathan.doye@chem.ox.ac.uk

Abstract: Molecular simulations using coarse-grained models allow the structure, dynamics and mechanics of DNA origamis to be comprehensively characterized. Here, we focus on the free-energy landscape of a jointed DNA origami that has been designed to exhibit two mechanically stable states and for which a bistable landscape has been inferred from ensembles of structures visualized by electron microscopy. Surprisingly, simulations using the oxDNA model predict that the defect-free origami has a single free-energy minimum. The expected second state is not stable because the hinge joints do not simply allow free angular motion but instead lead to increasing free-energetic penalties as the joint angles relevant to the second state are approached. This raises interesting questions about the cause of this difference between simulations and experiment, such as how assembly defects might affect the ensemble of structures observed experimentally.

Keywords: DNA nanotechnology; DNA origami; free-energy landscape; molecular dynamics; coarse-grained modelling; umbrella sampling



Citation: Wong, C.K.; Doye, J.P.K. The Free-Energy Landscape of a Mechanically Bistable DNA Origami. *Appl. Sci.* **2022**, *12*, 5875. <https://doi.org/10.3390/app12125875>

Academic Editor:
Alexander E. Marras

Received: 21 January 2022

Accepted: 6 June 2022

Published: 9 June 2022

Publisher's Note: MDPI stays neutral with regard to jurisdictional claims in published maps and institutional affiliations.



Copyright: © 2022 by the authors. Licensee MDPI, Basel, Switzerland. This article is an open access article distributed under the terms and conditions of the Creative Commons Attribution (CC BY) license (<https://creativecommons.org/licenses/by/4.0/>).

1. Introduction

The DNA origami technique [1,2] has emerged as a powerful approach to create self-assembled nanostructures and nanodevices. The potential applications of origami structures include nanofabrication, nanophotonics and nanoelectronics, multi-functional materials, catalysis, molecular machines, biosensing, drug delivery and biophysics [3–6]. One area of increasing interest is their use as nanoscale mechanical devices [7]. In this field of DNA “mechanotechnology” [8] DNA constructs are used to generate [9–11], transmit [12] and sense [13] nanoscale forces. One approach is through the use of flexible DNA origami that can undergo large-scale structural changes [14–16]; for example, an externally-actuated shape change could be used to apply a force [17], or a force could be sensed through the change in structure it induces [18–20].

For such applications, it is important to fully understand the shape changes that origamis can undergo and how the thermodynamics and mechanics of these shape changes can be controlled through the origami design. In this regard, computational approaches have the potential to play an important role as they can provide direct insight into how the microscopic features of the design impact the overall properties of the origami [21–23].

Here, we explore these issues further by providing a detailed simulation analysis of the jointed DNA origami introduced by Zhou et al. [24] that is designed to be bistable with the free-energy barrier between the two stable states being a result of the internal mechanical stresses associated with intermediate states. Although this is a proof-of-principle example, the potential utility of nanodevices that can switch between conformations in response to some (environmental) perturbation is clear, for example, as biosensors. Observations of ensembles of origami structures by electron microscopy seem to have confirmed the essential bistability of the design. In particular, we will compute the free-energy landscape of this system and explore the role of the properties of the individual joints in determining

the overall behaviour. The study will raise interesting questions about the potential role of defects on the properties of these origami systems.

2. Materials and Methods

To model the DNA nanostructures we used the oxDNA coarse-grained model [25–27]. In particular, we used the second version of the model that has been fine-tuned to improve the modelling of origami structure [27]. As a result of its accurate description of the structural [28] and mechanical [29] properties of DNA origami, it has been widely used in the field of DNA nanotechnology, particularly to describe origamis with increasingly functionally complex properties that are otherwise hard to predict [11,30–36]. The oxDNA model is particularly well-suited to study jointed origami, as it can also capture the important local features of the junction, e.g., an accurate description of the mechanical properties of single-stranded DNA [26] is important to model the role of the single-stranded linkers on joint flexibility. Furthermore, oxDNA is computationally efficient enough to be combined with techniques such as umbrella sampling [37] and metadynamics [38] to compute the free-energy landscapes associated with mechanical deformations of DNA origamis.

In the oxDNA model, each nucleotide is represented by a rigid body. The nucleotides interact through a pairwise potential which has terms representing backbone connectivity, excluded-volume interactions, hydrogen bonding between base pairs, stacking interactions, and electrostatic interactions between backbone phosphate groups. Solvent is modelled implicitly as a dielectric continuum, and a Debye–Hückel approach is used to describe the electrostatic interactions. We choose to use an ionic strength corresponding to a salt concentration of $[\text{Na}^+] = 1.0 \text{ M}$, which is representative of the high salt conditions typically used for DNA nanotechnology.

The oxDNA simulation code was used to perform molecular dynamics simulations in the canonical ensemble, in particular making use of its GPU implementation [39]. To sample the free-energy landscapes we used umbrella sampling in a similar manner to our previous work [37]. For each free-energy landscape we ran a series of between 20 and 80 simulations each of which sampled a separate order-parameter window due to the placement of a harmonic biasing potential in the order parameter at the centre of the window. The free-energy landscapes were constructed from the order-parameter probability distributions for each window using the weighted-histogram analysis method (WHAM) [40]. We iterated the sets of umbrella sampling simulations until the WHAM-generated landscapes no longer changed significantly.

Additional simulation and analysis details can be found in the Supplementary Material.

3. Results

3.1. Origami Design and Structure

The bistable jointed origami consists of four rod-like blocks of parallel double helices based on a hexagonal lattice that are linked through scaffold connections forming a roughly planar arrangement (Figure 1). In Ref. [24] these blocks have been termed the frame (dark blue), compliant (red), crank (green) and coupler (cyan) blocks. The central section of the compliant block is a 6-helix bundle and is designed to bend more easily than the other blocks which are all based on 10-helix bundles. For example, using the oxDNA model such a 10-helix bundle has been found to have a bending persistence length that is about three times larger than a 6-helix bundle [29].

Joint 1 between the frame and compliant block is designed to be rigid, whereas joints 2–4 are designed to behave like hinges allowing free rotational motion of the blocks in the plane of the structure. Joints 2 and 3 are connected by short single-stranded linkers on one side of the block, so that the block can rotate about that edge. The linkers for joint 4 are somewhat longer to provide additional flexibility so that the joint can bend both inwards and outwards.

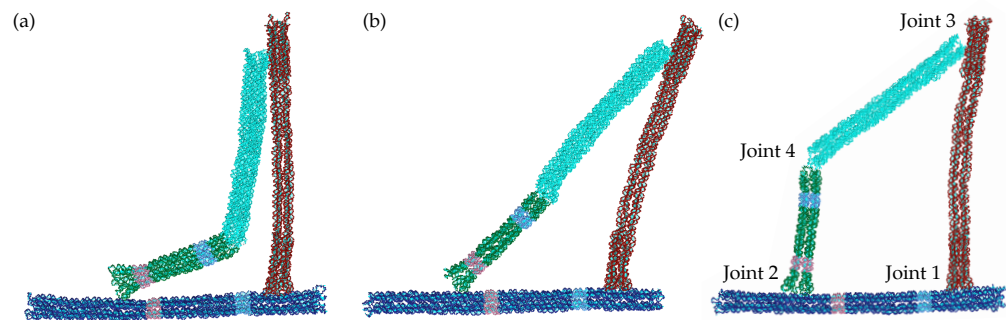


Figure 1. Representative oxDNA configurations of the origami in (a) the closed state S1 ($\theta \approx 20^\circ$) (b) the intermediate state U ($\theta \approx 45^\circ$) and (c) the open state S2 ($\theta \approx 80^\circ$). The four joints are numbered in (c).

The origami has been designed to have a free-energy landscape with two minima (termed the “closed” state S1 and the “open” state S2) as a function of θ the angle between the crank and the frame. Since joint 1 is rigid, in order for the origami to transition between the two stable states, the compliant block needs to bend outwards to accommodate the extra length between the ends of the crank and the coupler blocks. When the crank and the coupler blocks are collinear, the bending in the compliant block is at its maximum, and so this intermediate state U is expected to be unstable, i.e., a local maximum on the free-energy landscape. A simple mechanical model that accounts for the cost of bending the compliant block, while assuming free rotation at joints 2–4 predicts a free-energy barrier of $3\text{--}4 k_B T$ [24]. Representative oxDNA configurations at the θ values corresponding to S1, U and S2 are depicted in Figure 1; the substantial bending of the compliant block in the intermediate state U is very apparent, but it is interesting to note that in the open state some bending of this block still remains.

Experimentally, the free-energy landscape for this origami has been inferred from ensembles of structures visualized using electron microscopy [24]. In particular, the probability distribution for θ was measured (the free-energy landscape is proportional to the log of this distribution). The main peaks at 28° and 80° correspond to states S1 and S2, but surprisingly there was a small sub-peak in the probability distribution at intermediate values of θ rather than a minimum. It was suggested that this sub-population in the U state might be a result of coaxial stacking between the ends of the crank and coupler blocks when they are collinear.

3.2. Free-Energy Landscape

The free-energy landscape was calculated using umbrella sampling and WHAM. We chose the order parameter in the umbrella potential as the distance R between the centres of mass of two groups of nucleotides in the crank block and the frame block, respectively. The groups of nucleotides are highlighted in Figure 2a. We chose to use R as the order parameter rather than θ because calculating the forces on the nucleotides due to the umbrella potential is then much simpler and had already been implemented in the oxDNA simulation code [37]. The values of R and θ were tracked during the umbrella sampling simulations so that we can then transform the free-energy landscape from a function of R to a function of θ . The resulting landscape is shown in Figure 2b.

Contrary to previous expectations, the landscape obtained using the oxDNA model only shows a single minimum at $\theta \approx 80^\circ$, which corresponds to state S2. There is no sign of any second minimum corresponding to state S1. Instead, the free energy continuously increases as θ decreases. At $\theta \approx 20^\circ$, where state S1 is expected to occur, the free energy is more than $20 k_B T$. This is significantly different from the expectation based on the experimental results, where about 30% of the origamis were observed to be in the closed state.

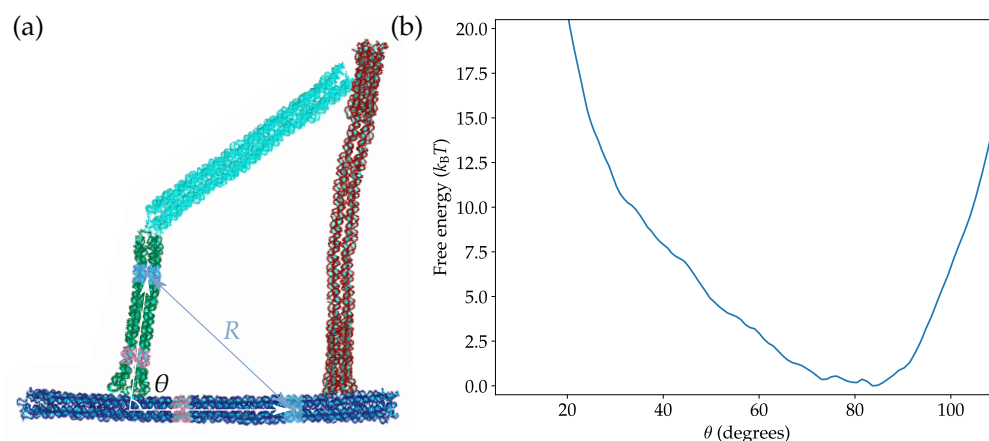


Figure 2. (a) A configuration of the origami illustrating the definition of the order parameter R as the distance between the centres of mass of the two groups of nucleotides coloured in light blue. The value of θ was tracked in the simulations, and is defined as the angle between the two vectors coloured in white. The vectors pass through the centres of mass of the two groups of nucleotides coloured in light red and light blue in the crank block and the frame block, respectively. (b) The free-energy landscape of the origami as a function of θ at $T = 300$ K.

Given the seeming disagreement between the obtained free-energy landscape and the experimental results, we further explored the dependence of the landscape on the solution conditions and temperature. Given the relative simplicity of the description of ionic interactions in the oxDNA model, we first checked that the destabilization of the closed state is not due to an overly strong electrostatic contribution to interhelical repulsions [41]. We found that even when the electrostatic interactions were tuned off, the landscape still had a single free-energy minimum corresponding to the open state (Figure S1). Secondly, we explored the temperature dependence of the free-energy landscape but found that there was little discernible change over the 40 K window that we considered (Figure S2). These results confirm that the single-minimum character of the free-energy landscape is a robust feature of the oxDNA simulations.

3.3. Free-Energy Decomposition

To better understand the form of the oxDNA free-energy landscape, and in particular why there is no minimum corresponding to state S1, we attempted to compute the contributions to the free-energy landscape from the four joints. In the complete origami the motion of the four joints is coupled due to the overall structure of the origami. Therefore, to isolate the behaviour of the individual joints we performed a series of simulations with one or more blocks of the origami removed (see the configurations in Figure 3). Similar to the previous section, we then defined distance order parameters between the centres of mass of groups of nucleotides to probe the motion of a given joint. The definitions of the order parameters and their respective free-energy landscapes are shown in Figure 3.

Joint 1 is designed to be rigid and, as expected, the free-energy minimum is when the frame and compliant blocks are perpendicular and unbent. The free-energy cost of changing the distance order parameter comes mainly from the bending of the compliant block instead of a change in the angle at the joint. This degree of freedom is the intended mode of stress accumulation in the original design that leads to disfavouring of the intermediate state.

Joints 2 and 3 are both designed to act as hinges and have a similar local structure. However, as their free-energy landscapes show, the hinges are not completely flexible. They have preferred opening angles at around 55° and 70° , respectively, and there is a non-negligible free-energy cost when the angles deviate from the preferred values. In particular, there are significant steric repulsions between the helices in the two blocks when the opening angle goes beyond 90° or approaches zero.

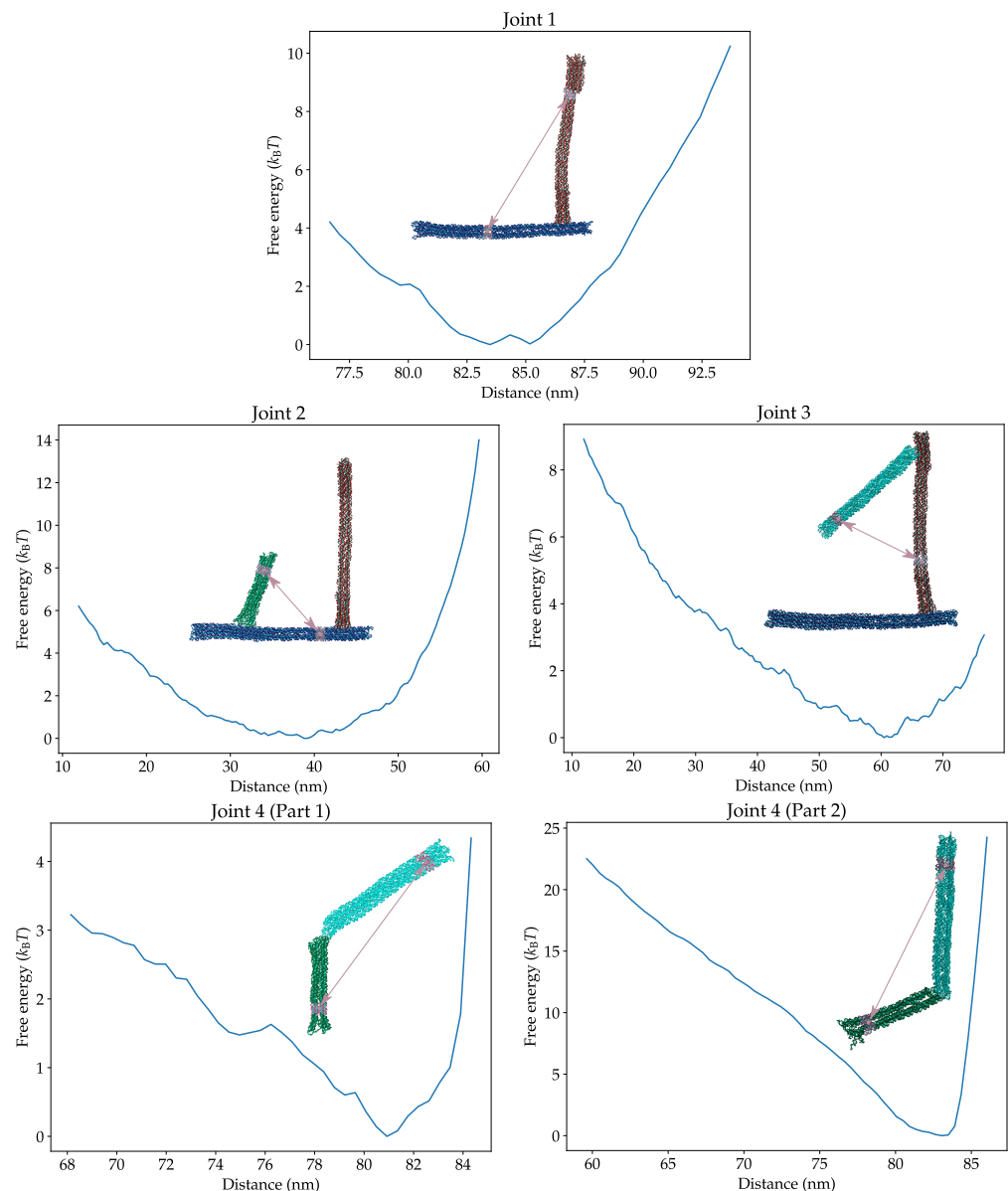


Figure 3. The free-energy landscapes associated with each individual joint. The configurations illustrate the subsystems used to compute these landscapes and the definitions of the distance order parameters. The values of these order parameters in the depicted configurations are 86 nm, 45 nm, 51 nm, 78 nm and 70 nm, respectively. The landscape associated with joint 4 has been computed in two parts corresponding to whether the joint is pointing outwards (1) or inwards (2). Only when joint 4 is straight do these sub-landscapes sample equivalent configurations.

Joint 4 was designed to be more flexible as the joint needs to bend both inward and outward to allow both the open and closed states to be easily accessed. The landscape for the joint has been computed in two sections because the distance order parameter on its own cannot distinguish whether the interior angle of the joint is obtuse (as in the open state) or reflex (as in the closed state). We find that the joint prefers to be roughly straight with an increasing free-energy penalty for more bent configurations; we note that we do not observe any coaxial stacking between the helix ends either side of the joint even when it adopts a straight configuration. (Note that the sharp rise in the free energy at large values of the distance order parameter is due to the stretching of the straight joint and is not relevant to the behaviour of the complete origami.) Particularly noteworthy is the asymmetry between bending the junction outwards and inwards, with a much higher cost

for the inward bending due to the resulting steric repulsions between the helices near to the joint (Figure 4).

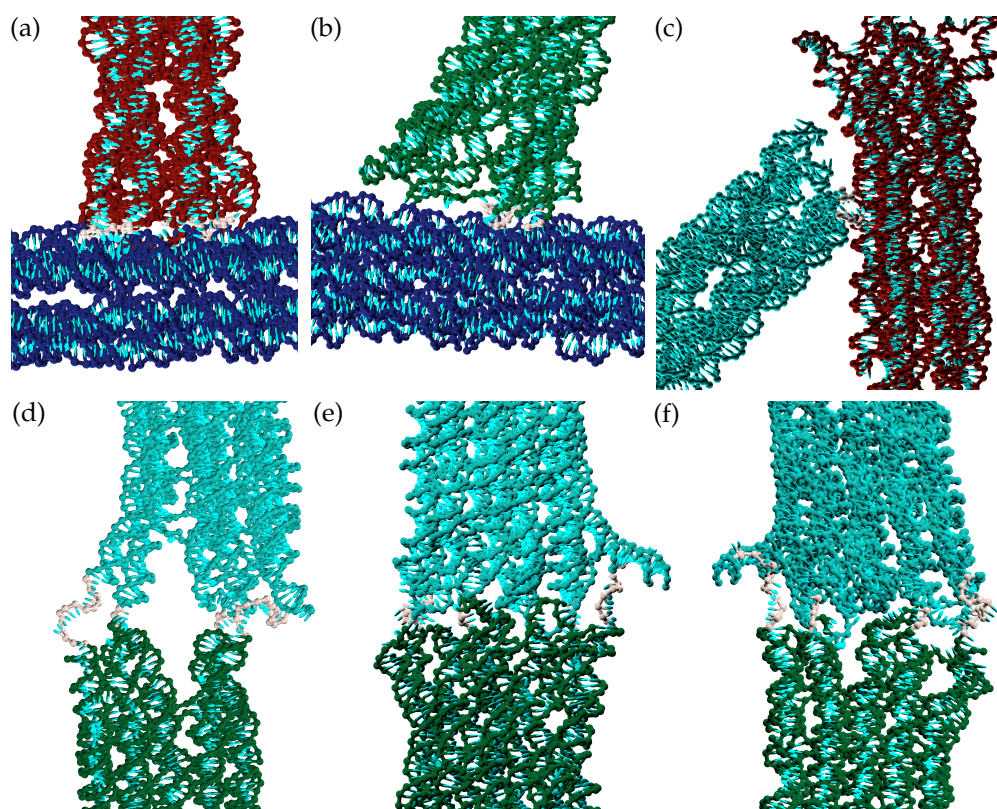


Figure 4. Close-ups of each joint for the configurations illustrated in Figure 3. Specifically, these are for (a) Joint 1 (b) Joint 2 (c) Joint 3 (d) Joint 4 (part 1) (e) Joint 4 (part 2, view from outside) (f) Joint 4 (part 2, view from inside). (The outside and inside of joint 4 are defined relative to the quadrilateral formed by the four blocks.) Single-stranded sections of the scaffold that link the blocks are coloured grey. (d–f) clearly show the difference in steric repulsion between the helices near the joint for open and closed configurations of joint 4.

By keeping track of the distance order parameters of each joint as well as R and θ in the simulations of the complete origami, we can transform the free-energy landscapes of the individual joints to be functions of θ (Figure S1). We next check if the free energy of the complete origami where the motion of the joints is coupled can be represented as the sum of the contributions from the individual joints. The comparison in Figure 5 shows that this is a very good approximation. Having established this, we now use these landscapes to understand why oxDNA predicts the closed state S1 to be unstable.

The contribution to the free energy of the complete origami associated with joint 1 shows two minima at $\theta \approx 20^\circ$ and at $\theta \approx 90^\circ$, and a maximum at around $\theta \approx 45^\circ$ (Figure 6). These positions generally agree with the angles for the S1, U and S2 states observed experimentally [24]. Furthermore, this component of the free-energy landscape is very similar to that predicted by the mechanical model used in that paper, albeit with a slightly larger barrier that is probably due to the somewhat high values of persistence lengths that oxDNA predicts for DNA origami [29]. These results indicate that the designed mechanism for stress accumulation due to bending of the compliant block can be captured by oxDNA.

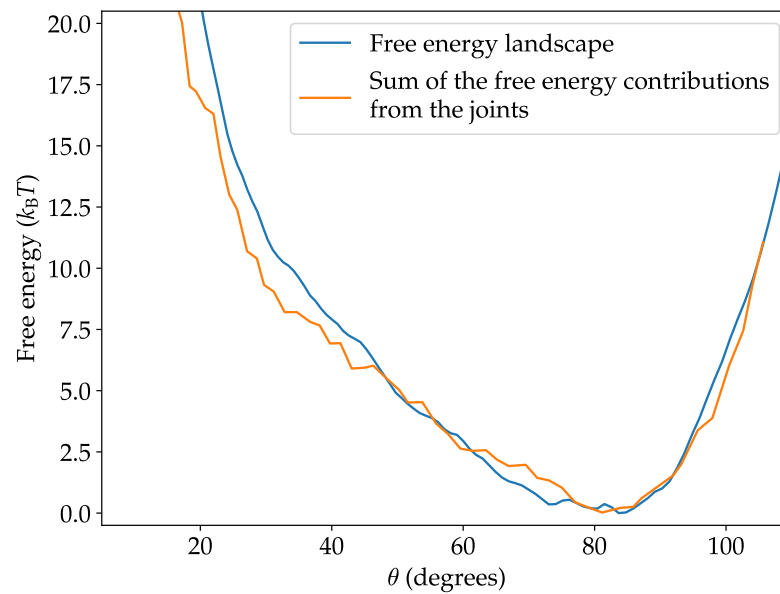


Figure 5. Comparison of the free-energy landscape and the sum of the contributions from the joints.

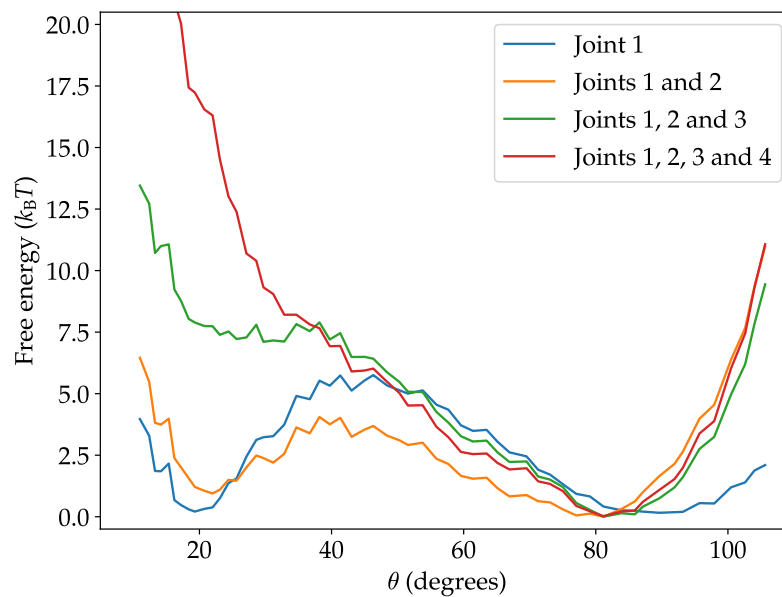


Figure 6. The Free-energy contributions of each joint to the overall free-energy landscape.

The free-energy contribution of joint 2 is a broad minimum centred around the preferred opening angle of the joint (Figure S1), and so adding this contribution does not significantly alter the general shape of the landscape. It slightly lowers the barrier and penalizes configurations with more extreme values of θ , particularly those with $\theta > 90^\circ$, because of the steric repulsions between the crank and frame blocks at these joint angles.

Further including the contribution from joint 3 results in an appreciable change in the shape of the landscape. Most noticeably, the minimum corresponding to S1 becomes a flat region with a higher free energy. The contribution of joint 3 has a more significant effect than joint 2 because the structure of the origami necessitates smaller opening angles at joint 3 than joint 2. It is these small opening angles, and their associated free-energy cost, that particularly lead to the destabilization of S1.

Finally, including the contribution from joint 4 completely removes the second minimum, because the inward bending of this joint that is associated with the closed configuration leads to a significantly larger free-energy cost.

4. Discussion

In this paper, we used the oxDNA coarse-grained model to compute the free-energy landscape of a jointed multi-block DNA origami that was designed to have two stable states. Somewhat surprisingly, the oxDNA landscape shows a single minimum corresponding to the open configuration. These results present a substantially different picture of the landscape to that inferred from experiment for which a significant population of origami in the closed state was observed.

The bending of the compliant block associated with intermediate configurations, leads to a bistable landscape associated with joint 1, as intended in the origami design. However, the other three joints do not behave like completely free hinges in oxDNA and this leads to the destabilization of the closed state with the small opening angles at joint 3 and the inward bending of joint 4 being particularly unfavourable. The increase in the free energy of the hinge joints as their joint angles move away from their preferred values is due both to direct steric repulsions and the constraints increasingly placed on the configuration of the helices and linkers near the joint. We note that these effects are consistent with previous oxDNA results on jointed DNA nanostructures [22,23] that have also found narrower distributions for the flexible components than observed in electron microscopy images; i.e., joints in oxDNA seem to be less flexible than inferred from experiment.

So, what are the possible causes of the seeming disagreement between the simulations and experiment? One possibility is simply that the oxDNA model is deficient in its description of these structures. However, the behaviour of the joints must be a reflection of the structural and mechanical properties of the helices and single-stranded DNA at the joints, which are all things that oxDNA describes well. Moreover, these are not small effects; oxDNA is predicting that the closed state of the origami is $20 k_B T$ higher in energy than the open state.

Another possible source is the heterogeneity in the ensemble of assembled origami in experiment. Whereas the simulations model a defect-free origami, there are likely to be a range of assembly and other defects in the experimental origami. These assembly defects probably not only include missing staples but also defects in the routing of the strands. The latter may be particularly relevant to multi-block origami, such as those studied here, which possess many scaffold links between the blocks. For example, if the blocks nucleate and assemble independently [42], then if the assembly of one block happens to lead to the topological entanglement of the external scaffold loops, such a defect is likely to be locked in. Furthermore, the assembly of further blocks might push these defects to the joints, potentially substantially changing the properties of the joint. Although there has been some quantification of missing staples [43–45], there is little information about other possible defects. Thus, it is conceivable that the population of closed configuration corresponds to origami that are locked into this structure due to assembly defects or that have more flexible joints due to missing staples.

There is some evidence of this heterogeneity in the experimental results. For example, it is not clear why there was a small sub-population of U states even though such structures were designed to be at a maximum on the free-energy landscape. Again, it is possible that they might be locked in to these configurations by defects. Furthermore, that a fraction of the open configurations do not close on the addition of actuating strands that lead to binding between the frame and crank blocks, and the coupler and compliant blocks again suggests the presence of certain defects preventing the closing.

One possible way to help address these issues and to quantify the heterogeneity in such ensembles of flexible origamis might be to use single-molecule techniques that can follow the large-scale dynamical motion of individual origami. For example, recent single-molecular FRET experiments on a two-block DNA origami nanohinge was able to observe fluctuations between open and closed states driven by the hybridization and melting of complementary strands attached to each block [46]. However, it is noteworthy that only a relatively small sub-population of the origamis (13% averaged across measurements for all hinge designs) were observed to undergo such fluctuations. Simulations could also be

used to investigate these questions by, for example, exploring the effects of different types of defects on origami properties.

Supplementary Materials: The following supporting information can be downloaded at: <https://www.mdpi.com/article/10.3390/app12125875/s1>, Section S1: Further results, Section S2: Simulation details. Refs. [47–50] are list in this part.

Author Contributions: Conceptualization, J.P.K.D.; methodology, C.K.W.; investigation, C.K.W.; writing—original draft preparation, J.P.K.D. and C.K.W.; writing—review and editing, J.P.K.D. and C.K.W.; supervision, J.P.K.D. All authors have read and agreed to the published version of the manuscript.

Funding: This research was funded by the Croucher Foundation.

Institutional Review Board Statement: Not applicable.

Informed Consent Statement: Not applicable.

Data Availability Statement: The data presented in this study is available at the Oxford University Research Archive (<https://ora.ox.ac.uk/objects/uuid:3cd5f7b9-f86d-45b0-a68b-a1d2acb14a38>, accessed on 20 January 2022).

Acknowledgments: The authors acknowledge the use of the University of Oxford Advanced Research Computing (ARC) facility (<http://dx.doi.org/10.5281/zenodo.22558>) (accessed on 20 January 2022).

Conflicts of Interest: The authors declare no conflict of interest.

References

1. Rothmund, P.W.K. Folding DNA to create nanoscale shapes and patterns. *Nature* **2006**, *440*, 297–302. [CrossRef]
2. Douglas, S.M.; Dietz, H.; Liedl, T.; Högberg, B.; Graf, F.; Shih, W.M. Self-assembly of DNA into nanoscale three-dimensional shapes. *Nature* **2009**, *459*, 414–418. [CrossRef]
3. Wang, P.; Meyer, T.A.; Pan, V.; Dutta, P.K.; Ke, Y. The beauty and utility of DNA origami. *Chem* **2017**, *2*, 359–382. [CrossRef]
4. Tapio, K.; Bald, I. The potential of DNA origami to build multifunctional materials. *Multifunct. Mater.* **2020**, *3*, 032001. [CrossRef]
5. Dey, S.; Fan, C.; Gothelf, K.V.; Li, J.; Lin, C.; Liu, L.; Liu, N.; Nijenhuis, M.A.D.; Sacca, B.; Simmel, F.C.; et al. DNA origami. *Nat. Rev. Methods Prim.* **2021**, *1*, 13. [CrossRef]
6. Engelen, W.; Dietz, H. Advancing biophysics using DNA origami. *Annu. Rev. Biophys.* **2021**, *50*, 469–492. [CrossRef] [PubMed]
7. DeLuca, M.; Shi, Z.; Castro, C.E.; Arya, G. Dynamic DNA nanotechnology: Toward functional nanoscale devices. *Nanoscale Horiz.* **2020**, *5*, 182–201. [CrossRef]
8. Blanchard, A.T.; Salaita, K. Emerging uses of DNA mechanical devices. *Science* **2019**, *365*, 1080–1081. [CrossRef] [PubMed]
9. Nickels, P.C.; Wunsch, B.; Holzmeister, P.; Bae, W.; Kneer, L.M.; Grohmann, D.; Tinnefeld, P.; Liedl, T. Molecular force spectroscopy with a DNA origami-based nanoscopic force clamp. *Science* **2016**, *354*, 305–307. [CrossRef] [PubMed]
10. Le, J.V.; Luo, Y.; Darcy, M.A.; Lucas, C.R.; Goodwin, M.F.; Poirier, M.G.; Castro, C.E. Probing nucleosome stability with a DNA origami nanocaliper. *ACS Nano* **2016**, *10*, 7073–7084. [CrossRef] [PubMed]
11. Su, H.; Brockman, J.M.; Duan, Y.; Sen, N.; Chhabra, H.; Bazrafshan, A.; Blanchard, A.T.; Meyer, T.; Andrews, B.; Doye, J.P.K.; et al. Massively parallelized molecular force manipulation with on demand thermal and optical control. *J. Am. Chem. Soc.* **2021**, *43*, 19466–19473. [CrossRef]
12. Pfitzner, E.; Wachauf, C.; Kilchherr, F.; Pelz, B.; Shih, W.M.; Rief, M.; Dietz, H. Rigid DNA beams for high-resolution single-molecule mechanics. *Angew. Chem. Int. Ed.* **2013**, *52*, 7766–7771. [CrossRef]
13. Dutta, P.K.; Zhang, Y.; Blanchard, A.T.; Ge, C.; Rushdi, M.; Weiss, K.; Zhu, C.; Ke, Y.; Salaita, K. Programmable multi-valent DNA-origami tension probes for reporting cellular traction forces. *Nano Lett.* **2018**, *18*, 4803–4811. [CrossRef]
14. Zhou, L.; Marras, A.E.; Castro, C.E. Origami Compliant Nanostructures with Tunable Mechanical Properties. *ACS Nano* **2014**, *8*, 27–34. [CrossRef]
15. Marras, A.E.; Zhou, L.; Su, H.J.; Castro, C.E. Programmable Motion of DNA Origami Mechanisms. *Proc. Natl. Acad. Sci. USA* **2015**, *112*, 713–718. [CrossRef]
16. Zhou, L.; Marras, A.E.; Huang, C.M.; Castro, C.E.; Su, H.J. Paper origami-inspired design and actuation of DNA nanomachines with complex motions. *Small* **2018**, *14*, 1802580. [CrossRef]
17. Wang, Y.; Le, J.V.; Crocker, K.; Darcy, M.A.; Halley, P.D.; Zhao, D.; Andrioff, N.; Croy, C.; Poirier, M.G.; Bundschuh, R.; et al. A nanoscale DNA force spectrometer capable of applying tension and compression on biomolecules. *Nucleic Acids Res.* **2021**, *49*, 8987–8999. [CrossRef]
18. Funke, J.J.; Ketterer, P.; Lieleg, C.; Schunter, S.; Korber, P.; Dietz, H. Uncovering the forces between nucleosomes using DNA origami. *Sci. Adv.* **2016**, *2*, e1600974. [CrossRef]

19. Hudoba, M.W.; Luo, Y.; Zacharias, A.; Poirier, M.G.; Castro, C.E. Dynamic DNA origami device for measuring compressive depletion forces. *ACS Nano* **2017**, *11*, 6566–6573. [\[CrossRef\]](#)
20. Ke, Y.; Meyer, T.; Shih, W.M.; Bellot, G. Regulation at a distance of biomolecular interactions using a DNA nanoactuator. *Nat. Commun.* **2016**, *7*, 10935. [\[CrossRef\]](#)
21. Shi, Z.; Castro, C.E.; Arya, G. Conformational dynamics of mechanically compliant DNA nanostructures from coarse-grained molecular dynamics simulations. *ACS Nano* **2017**, *11*, 4617–4630. [\[CrossRef\]](#)
22. Sharma, R.; Schreck, J.S.; Romano, F.; Louis, A.A.; Doye, J.P.K. Characterizing the Motion of Jointed DNA Nanostructures Using a Coarse-Grained Model. *ACS Nano* **2017**, *11*, 12426–12435. [\[CrossRef\]](#)
23. Shi, Z.; Arya, G. Free Energy Landscape of Salt-Actuated Reconfigurable DNA Nanodevices. *Nucleic Acids Res.* **2019**, *48*, 548–560. [\[CrossRef\]](#)
24. Zhou, L.; Marras, A.E.; Su, H.J.; Castro, C.E. Direct Design of an Energy Landscape with Bistable DNA Origami Mechanisms. *Nano Lett.* **2015**, *15*, 1815–1821. [\[CrossRef\]](#)
25. Ouldrige, T.E.; Louis, A.A.; Doye, J.P.K. Structural, Mechanical, and Thermodynamic Properties of a Coarse-Grained DNA Model. *J. Chem. Phys.* **2011**, *134*, 085101. [\[CrossRef\]](#)
26. Šulc, P.; Romano, F.; Ouldrige, T.E.; Rovigatti, L.; Doye, J.P.K.; Louis, A.A. Introducing Sequence-Dependent Interactions into a Coarse-Grained DNA Model. *J. Chem. Phys.* **2012**, *137*, 135101. [\[CrossRef\]](#)
27. Snodin, B.E.K.; Randisi, F.; Mosayebi, M.; Šulc, P.; Schreck, J.S.; Romano, F.; Ouldrige, T.E.; Tsukanov, R.; Nir, E.; Louis, A.A.; et al. Introducing Improved Structural Properties and Salt Dependence into a Coarse-Grained Model of DNA. *J. Chem. Phys.* **2015**, *142*, 234901. [\[CrossRef\]](#)
28. Snodin, B.E.K.; Schreck, J.S.; Romano, F.; Louis, A.A.; Doye, J.P.K. Coarse-grained modelling of the structural properties of DNA origami. *Nucleic Acids Res.* **2019**, *47*, 1585–1597. [\[CrossRef\]](#)
29. Chhabra, H.; Mishra, G.; Cao, Y.; Prešern, D.; Skoruppa, E.; Tortora, M.M.C.; Doye, J.P.K. Computing the elastic mechanical properties of rod-like DNA nanostructures. *J. Chem. Theory Comput.* **2020**, *16*, 7748–7763. [\[CrossRef\]](#)
30. Benson, E.; Mohammed, A.; Rayneau-Kirkhope, D.; Gådin, A.; Orponen, P.; Högberg, B. Effects of design choices on the stiffness of wireframe DNA origami structures. *ACS Nano* **2018**, *12*, 9291–9299. [\[CrossRef\]](#) [\[PubMed\]](#)
31. Berengut, J.F.; Berengut, J.C.; Doye, J.P.K.; Prešern, D.; Kawamoto, A.; Ruan, J.; Wainwright, M.J.; Lee, L.K. Design and synthesis of pleated DNA origami nanotubes with adjustable diameters. *Nucleic Acids Res.* **2019**, *47*, 11963–11975. [\[CrossRef\]](#) [\[PubMed\]](#)
32. Berengut, J.F.; Wong, C.; Berengut, J.C.; Doye, J.P.K.; Ouldrige, T.E.; Lee, L.K. Self-limiting polymerization of DNA origami subunits with strain accumulation. *ACS Nano* **2020**, *14*, 17428–17441. [\[CrossRef\]](#) [\[PubMed\]](#)
33. Engel, M.C.; Romano, F.; Louis, A.A.; Doye, J.P.K. Measuring internal forces in single-stranded DNA: Application to a DNA force clamp. *J. Chem. Theory Comput.* **2020**, *16*, 7764–7775. [\[CrossRef\]](#)
34. Yao, G.; Zhang, F.; Wang, F.; Peng, T.; Liu, H.; Poppleton, E.; Šulc, P.; Jiang, S.; Liu, L.; Gong, C.; et al. Meta-DNA structures. *Nat. Chem.* **2020**, *12*, 1067–1075. [\[CrossRef\]](#)
35. Huang, C.M.; Kucinic, A.; Johnson, J.A.; Su, H.J.; Castro, C.E. Integrated computer-aided engineering and design for DNA assemblies. *Nat. Mater.* **2021**, *20*, 1264–1271. [\[CrossRef\]](#)
36. Li, R.; Chen, H.; Lee, H.; Choi, J.H. Elucidating the mechanical energy for cyclization of a DNA origami tile. *Appl. Sci.* **2021**, *11*, 2357. [\[CrossRef\]](#)
37. Wong, C.K.; Tang, C.; Schreck, J.S.; Doye, J.P.K. Characterizing the free-energy landscapes of DNA origamis. *Nanoscale* **2022**, *14*, 2638–2648. [\[CrossRef\]](#)
38. Kaufhold, W.T.; Pfeifer, W.; Castro, C.E.; Di Michele, L. Probing the mechanical properties of DNA nanostructures with metadynamics. *ACS Nano* **2022**, *16*. [\[CrossRef\]](#)
39. Rovigatti, L.; Šulc, P.; Reguly, I.Z.; Romano, F. A Comparison between Parallelization Approaches in Molecular Dynamics Simulations on GPUs. *J. Comput. Chem.* **2015**, *36*, 1–8. [\[CrossRef\]](#)
40. Kumar, S.; Rosenberg, J.M.; Bouzida, D.; Swendsen, R.H.; Kollman, P.A. The Weighted Histogram Analysis Method for Free-Energy Calculations on Biomolecules. I. The Method. *J. Comput. Chem.* **1992**, *13*, 1011–1021. [\[CrossRef\]](#)
41. Hamilton, I.; Gebala, M.; Herschlag, D.; Russell, R. Direct measurement of interhelical DNA repulsion and attraction by quantitative cross-linking. *J. Am. Chem. Soc.* **2022**, *144*, 1718–1728. [\[CrossRef\]](#)
42. Marras, A.E.; Zhou, L.; Kolliopoulos, V.; Su, H.J.; Castro, C.E. Directing folding pathways for multi-component DNA origami nanostructures with complex topology. *New J. Phys* **2016**, *18*, 055005. [\[CrossRef\]](#)
43. Wagenbauer, K.F.; Wachauf, C.H.; Dietz, H. Quantifying quality in DNA self-assembly. *Nat. Commun.* **2014**, *5*, 3691. [\[CrossRef\]](#)
44. Myhrvold, C.; Baym, M.; Hanikel, N.; Ong, L.L.; Gootenberg, J.S.; Yin, P. Barcode extension for analysis and reconstruction of structures. *Nat. Commun.* **2017**, *8*, 14698. [\[CrossRef\]](#)
45. Strauss, M.T.; Scheuder, F.; Haas, D.; Nickels, P.C.; Jungmann, R. Quantifying absolute addressability in DNA origami with molecular resolution. *Nat. Commun.* **2018**, *9*, 1600. [\[CrossRef\]](#)
46. Darcy, M.; Crocker, K.; Wang, Y.; Le, J.V.; Mohammadiroozbahani, G.; Abdelhamid, A.S.; Craggs, T.D.; Castro, C.; Bundschuh, R.; Poirier, M.G. High-Force Application by a Nanoscale DNA Force Spectrometer. *ACS Nano* **2022**, *16*, 5682–5695. [\[CrossRef\]](#)
47. Suma, A.; Poppleton, E.; Matthies, M.; Šulc, P.; Romano, F.; Louis, A.A.; Doye, J.P.K.; Micheletti, C.; Rovigatti, L. TacoxDNA: A User-Friendly Web Server for Simulations of Complex DNA Structures, from Single Strands to Origami. *J. Comput. Chem.* **2019**, *40*, 2586–2595. [\[CrossRef\]](#)

-
48. Poppleton, E.; Bohlin, J.; Matthies, M.; Sharma, S.; Zhang, F.; Šulc, P. Design, optimization and analysis of large DNA and RNA nanostructures through interactive visualization, editing and molecular simulation. *Nucleic Acids Res.* **2020**, *48*, e72. [[CrossRef](#)]
 49. Torrie, G.; Valleau, J. Nonphysical Sampling Distributions in Monte Carlo Free-Energy Estimation: Umbrella sampling. *J. Comput. Phys.* **1977**, *23*, 187–199. [[CrossRef](#)]
 50. Grossfield, A. WHAM: The Weighted Histogram Analysis Method. Version 2.0.9. Available online: <http://membrane.urmc.rochester.edu/sites/default/files/wham/doc.pdf> (accessed on 20 January 2022).